TU Delft

Delft University of Technology

CFD based parametric investigations of film cooling effectiveness for various coolant injection hole geometries and injection angles

Jindal, Prakhar; Naagar, Manish; Krishna, S. M.Murali; Singholi, Ajay K.Singh

DOI
10.1007/s12046-024-02492-1

Publication date
2024

Document Version
Final published version

Published in
Sadhana - Academy Proceedings in Engineering Sciences

Citation (APA)
Jindal, P., Naagar, M., Krishna, S. M. M., & Singholi, A. K. S. (2024). CFD based parametric investigations of film cooling effectiveness for various coolant injection hole geometries and injection angles. *Sadhana - Academy Proceedings in Engineering Sciences*, *49*(2), Article 158. https://doi.org/10.1007/s12046-024-02492-1

Important note
To cite this publication, please use the final published version (if applicable).
Please check the document version above.

Copyright
Other than for strictly personal use, it is not permitted to download, forward or distribute the text or part of it, without the consent of the author(s) and/or copyright holder(s), unless the work is under an open content license such as Creative Commons.

Takedown policy
Please contact us and provide details if you believe this document breaches copyrights.
We will remove access to the work immediately and investigate your claim.

This work is downloaded from Delft University of Technology.
For technical reasons the number of authors shown on this cover page is limited to a maximum of 10.

Green Open Access added to TU Delft Institutional Repository

'You share, we take care!' - Taverne project

https://www.openaccess.nl/en/you-share-we-take-care

Otherwise as indicated in the copyright section: the publisher is the copyright holder of this work and the author uses the Dutch legislation to make this work public.

Sādhanā (2024) 49:158
https://doi.org/10.1007/s12046-024-02492-1
© Indian Academy of Sciences

CFD based parametric investigations of film cooling effectiveness for various coolant injection hole geometries and injection angles

PRAKHAR JINDAL[1,*], MANISH NAAGAR[2], S M MURALI KRISHNA[3] and AJAY K SINGH SINGHOLI[4]

[1]Space System Engineering, Faculty of Aerospace Engineering, TU Delft, Delft, The Netherlands
[2]Department of Aerospace Engineering, Amity University Haryana, Gurugram, India
[3]Vignan's Institute of Information Technology, Visakhapatnam, Andhra Pradesh, India
[4]University School of Automation and Robotics, Guru Gobind Singh Indraprastha University, New Delhi, Delhi, India
e-mail: p.jindal@tudelft.nl

MS received 1 May 2022; revised 17 August 2023; accepted 10 February 2024

Abstract. Computational analysis on film cooling effectiveness over a flat plate using different coolant injection hole geometries are reported. The designed computational setup and flow physics are suitably validated against the existing experimental results for an injection angle of 30°. The present study reports and compares the degree of film cooling effectiveness obtained by the different orientations of the coolant injection holes and their geometry, hole arrangements in the rows and number of rows. The computational domain was designed using Ansys Fluent. The blowing ratio is systematically ranged between 0.67 and 1.67. The performance of a given film cooling scheme is reported in terms of centreline (ηcl) and spatially averaged (η_{sa}) adiabatic effectiveness. It is observed that for single hole configuration, the semi-elliptic geometry increases the ηcl by ∼66.67% up to *x/D(ratio of downstream distance from hole to diameter of hole)* = 50 at lower blowing ratios (0.67 and 1.00) and by ∼50% up to *x/D*=100 at higher blowing ratios (1.33 and 1.67). For ηsa, an increment of ∼200% and ∼60% is achieved for all blowing ratios using the triangular and semi-elliptic geometries, respectively. For the multiple row arrangements, the two staggered rows delivered an increment in ηcl of ∼77% up to *x/D*=50 and ∼54% up to *x/D*=100. The two staggered configurations at 0° gave the highest effectiveness increment of ∼177% up to *x/D*=50 while it was ∼100% for up to *x/D*=100. Results indicate that the triangular geometry shows the highest values of the film cooling effectiveness, and a semi- elliptic geometry utilizes ∼50% of the coolant mass flow than other coolant injection hole geometries while delivering higher effectiveness values.

Keywords. CFD; blowing ratio; film cooling; coolant injection hole; film cooling effectiveness.

1. Introduction

The film cooling (FC) phenomena of any cooling scheme can be quantitatively expressed by measuring its film cooling effectiveness (η_{fc}), also called adiabatic film cooling effectiveness. Film cooling studies over an adiabatic flat plate typically involves an uninterrupted injection of a thin stream of coolant over the plate surface to provide insulation from the flowing high- temperature fluids [1]. The main advantages of using this FC technique in the combustion chamber of a liquid rocket engine are that it can lead to designing comparatively light-weight nozzle assemblies and is comparatively simpler to fabricate and operate. Mathematically, η_{fc} can be expressed as presented in equation 1 [2].

$$\eta_{fc} = \frac{T_\infty - T_w}{T_\infty - T_c} \tag{1}$$

The η_{fc} depends on the geometry of the coolant injection hole (CIH), CIH layout and arrangement, and the injection angle [3]. Researchers have extensively conducted computational and experimental studies on various FC techniques. Bunker [4], in his comprehensive review on FC from different CIHs geometries, concluded that no single geometry of CIHs delivers optimal performance over versatile application parameters. He also concluded that the CIH's geometry is a key parameter that governs the intensity of mixing, coolant film coverage and the vicinity of cooling jets to the surface. Goldstein *et al* [5] presented

*For correspondence
Published online: 25 April 2024

the effectiveness of a single cylindrical CIH and a row of cylindrical coolant injection holes. They reported achieving maximum η_{fc} at a blowing ratio (M) of 0.5 and a coolant to free-stream density ratio of 1.0.

Yuen and Martinez [6, 7] studied the heat transfer and film cooling effectiveness using a cylindrical CIH at injection angles of 30°, 60°, and 90°. They considered a CIH length-to-diameter (L/D) ratio of 4, the free-stream Reynolds number of 8563, and they systematically varied M from 0.33 to 2.0. They reported that the maximum η_{fc} increased up to M=0.5, then decreased with increasing M for a single 30° CIH. They attributed this behaviour to the occurrence of jet penetration into the free stream. Chen [8] studied the η_{fc} and heat transfer coefficients for rows of circular CIHs with different injection angles. Wang and Li [9] studied the film cooling performance by introducing a small quantity of water into the cooling air using Ansys Fluent. They conducted their investigations at a pressure and temperature of 15 atm and 1561 K, respectively. Their findings showed that a 5-10% increment in the cooling effectiveness can be achieved by using 10–20% of mist along with an added reduction of 30- 68 K adiabatic wall temperature. The influence of different CIH geometries on FC with CO2 was investigated by Guangchao *et al* [10]. Dellimore [11] reported the disparities in the literature about the influence of compressibility in film cooling effectiveness by providing its significant contribution of enhancing film cooling with a condition of high convective Mach numbers with low temperature ratio. Their results showed improvement in film cooling with decreasing total temperature ratio and increasing convective Mach number. Wright *et al* [12] experimentally investigated a 35° injection angle, with the M varying from 0.25 to 2.0. They varied the density ratio from 1.0 to 1.4, and their investigation revealed that η_{fc} values are directly proportional to the density ratio while inversely proportional to the blowing ratio. Baheri *et al* [13] reported the effect of L/D ratio with the trenched and cylindrical CIHs at M= 0.6 and 1.25, and an injection angle of 35°. Their study concluded that the averaged η_{fc} increased in direct proportion to the L/D ratio.

The available literature suggests that η_{fc} mainly depends on injection angle, blowing ratio, L/D ratio, and compound angle/orientation of the CIHs. Therefore, the current investigation aspires to study the effects of various CIH geometries and their different lateral orientations on the flow arrangement for a flat plate using the k-ε turbulence model. Available literature suggests that the k-ε turbulence model is best suited to study the mean flow over a flat plate [5, 9, 12, 13]. The novelty of this work includes the enhancement of cooling effectiveness with multiple hole shapes having constant inlet area, row arrangements at various blowing ratios and their evaluation with the state-of-the-art. Multiple computations are conducted for different CIH geometries, different numbers of rows with aligned and staggered CIHs configurations at different blowing ratios ranging from 0.67 to 1.67. The compound injection angles of the CIHs are also varied from 0° to 90°.

2. Methodology

2.1 *Mathematical model*

The steady-state heat transfer which is occurring in the flow on the geometrical surface are governed by the basic laws of physics and thermodynamics. The conservation laws of energy, mass, and momentum are well established in various open literatures. The related mathematical formulations can be found in this section later. The continuity (eq. 2), momentum (eq. 3-4), and energy (eq. 5) equations for the present case of steady-state, incompressible, segregated 3D solver, and standard k–ε (without viscous heating) turbulence model. Equation 6 represents the turbulent kinetic energy equation while eq. 7 presents the rate of dissipation of turbulent kinetic energy.

$$\frac{\partial u}{\partial x}+\frac{\partial u}{\partial y}=0 \tag{2}$$

$$u\frac{\partial u}{\partial x}+v\frac{\partial u}{\partial y}=-\frac{1}{\rho}\frac{\partial p}{\partial x}+\frac{\partial}{\partial x}\left(v\frac{\partial u}{\partial x}\right)+\frac{\partial}{\partial y}\left(v\frac{\partial u}{\partial y}\right)+f_1 \tag{3}$$

$$u\frac{\partial v}{\partial x}+v\frac{\partial v}{\partial y}=-\frac{1}{\rho}\frac{\partial p}{\partial y}+\frac{\partial}{\partial x}\left(v\frac{\partial v}{\partial x}\right)+\frac{\partial}{\partial y}\left(v\frac{\partial v}{\partial y}\right)+f_2 \tag{4}$$

$$\rho C_p\left(u\frac{\partial T}{\partial x}+v\frac{\partial T}{\partial y}\right)=\frac{\partial}{\partial x}\left(k\frac{\partial T}{\partial x}\right)+\frac{\partial}{\partial y}\left(k\frac{\partial T}{\partial y}\right)+Q \tag{5}$$

$$\frac{\partial \rho U_i k}{\partial x_j}=\mu_\tau\left(\frac{\partial U_i}{\partial x_j}+\frac{\partial U_j}{\partial x_i}\right)\frac{\partial U_i}{\partial x_j}+\frac{\partial}{\partial x_j}\left(\frac{\mu_\tau \partial k}{\sigma_k \partial x_j}\right)-\rho\varepsilon \tag{6}$$

$$\frac{\partial \rho U_j \varepsilon}{\partial x_j}=\mu_\tau C_1\frac{\varepsilon}{k}\left(\frac{\partial U_i}{\partial x_j}+\frac{\partial U_j}{\partial x_i}\right)\frac{\partial U_i}{\partial x_j}+\frac{\partial}{\partial x_j}\left(\frac{\mu_\tau \partial \varepsilon}{\sigma_\varepsilon \partial x_j}\right)-\rho C_2\frac{\varepsilon^2}{k} \tag{7}$$

2.1.1 *Physical model*

The computational domain was designed, and the mesh was generated using Ansys Fluent 14.1. The hot gases are simulated to pass over the flat plate surface, and the coolant is injected to generate a film between the surface and the high-temperature fluid. Figure 1 shows the schematic of the designed computational model. The coolant injection angle is 90°, and the compound angle is varied between 0° to 90°. The designed model is validated by comparing the obtained results for the performance of the cylindrical CIH with that of the results of the experimental investigations by Yuen *et al* [6]. The geometrical conditions are duplicated as reported in the literature to achieve a closer simulation. Investigations are also carried out on three other geometries of CIHs, i.e., semi-elliptic, and triangular, semi-cylindrical. The cross- sectional area of all the CIH geometries used in the present study is kept constant.

Figure 2 shows the schematic and modelled view of different CIH geometries and their orientations. Figure 2(a) shows a cross-sectional view of the geometrical model, while figure 2(b) shows the top as well as the

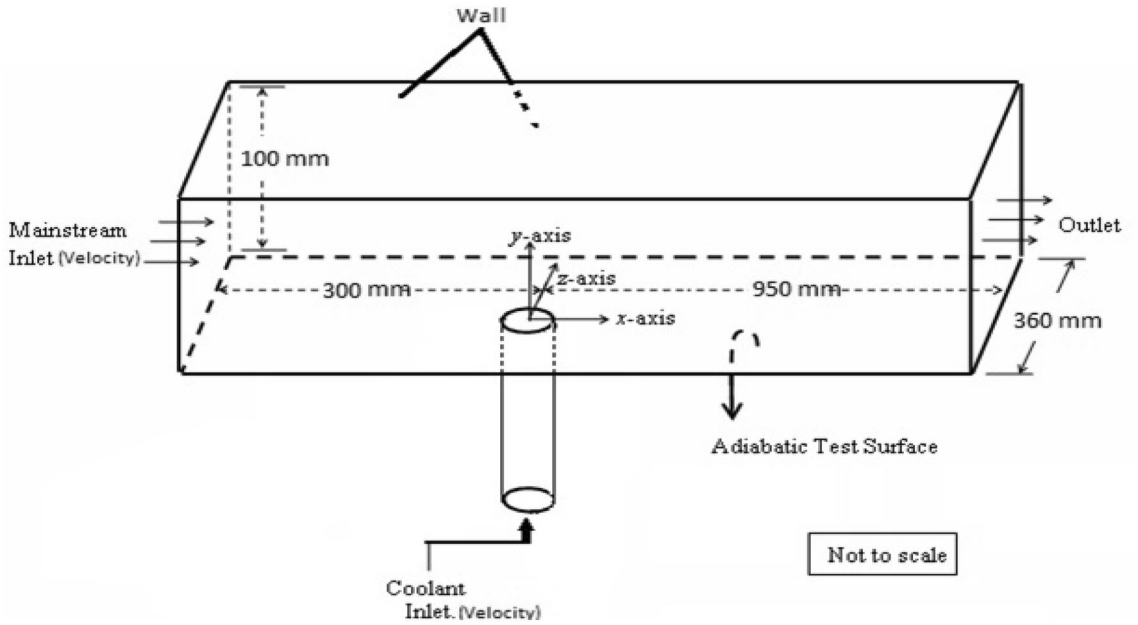

Figure 1. Cross-sectional view of designed computational model.

isometric view of the test plate with different CIH geometries. Figure 2(c) presents the model of two inline rows of CIHs, which have a row spacing of 100 mm. A streamwise distance of 100 mm was kept between two staggered rows of CIHs. The lateral distance between two consecutive CIHs from different rows and between CIHs of the individual row is kept as 50 mm and 35 mm, respectively. Figure 2(d) presents the models studied with different orientation angles (β) and the orientation angle is varied from 0° to 90°. Compound angles are made for each type of CIHs and their arrangement in the cases of rows.

2.2 *Boundary conditions*

The designed computational model, consisting of a cylindrical CIH, inclined at an angle of 30° streamwise with a diameter of 10 mm, is validated against the available experimental results. Table 1 reports the various boundary conditions of the designed simulation. Reynolds number, as governed by the free-stream velocity and CIH diameter, is 10364 and the *L/D* ratio of the CIH is kept as 7. The blowing ratio ranges from 0.67 to 1.67, corresponding to the coolant inlet velocities are presented in table 2.

2.3 *Solver*

A 3D segregated; steady-state solver is used for the present investigations. An implicit method is used for the linearization of governing equations. The k-ε model with standard wall functions for the plate cross-section area is used for the turbulence modelling. Enhanced wall treatment was avoided by designing the mesh fine enough to have the wall Y^+ values in the range of 0-5. The second-order upwind discretization scheme is used for turbulence kinetic energy, momentum, turbulence dissipation rate and energy, whereas a standard discretization scheme is used for the pressure [14]. Ansys Fluent 14.1 is used to obtain the solution of governing equations. Pressure–velocity coupling was done using a SIMPLE algorithm developed by Spalding and Patankar is used. The discretization scheme used was second-order upwind interpolation. Solution is continued till the residuals reached the convergence of 10^{-9} for energy, 10^{-6} for velocities, 10^{-6} for turbulence quantities. A user-defined function is used for plotting the ηcl values in all the cases.

2.4 *Grid independence test*

For the grid independence test, the cylindrical CIH at a blowing ratio of 1.0 is selected. Various grid sizes for different designed meshes are reported in table 3. Figure 3(a) represents the mesh independence for centerline film cooling effectiveness (ηcl). Figure 3(a) shows almost identical effectiveness values for different blowing ratios for different grid sizes. This is because these graphs are plotted only for a small number of points (21) extracted from a larger dataset. So, these are averaged values signifying the nature of curves rather than exact values. Figure 3(a) also shows that the results obtained from the medium and fine meshes are almost equivalent. However, the medium mesh is used for the investigation to obtain simulation results within a lesser computational time.

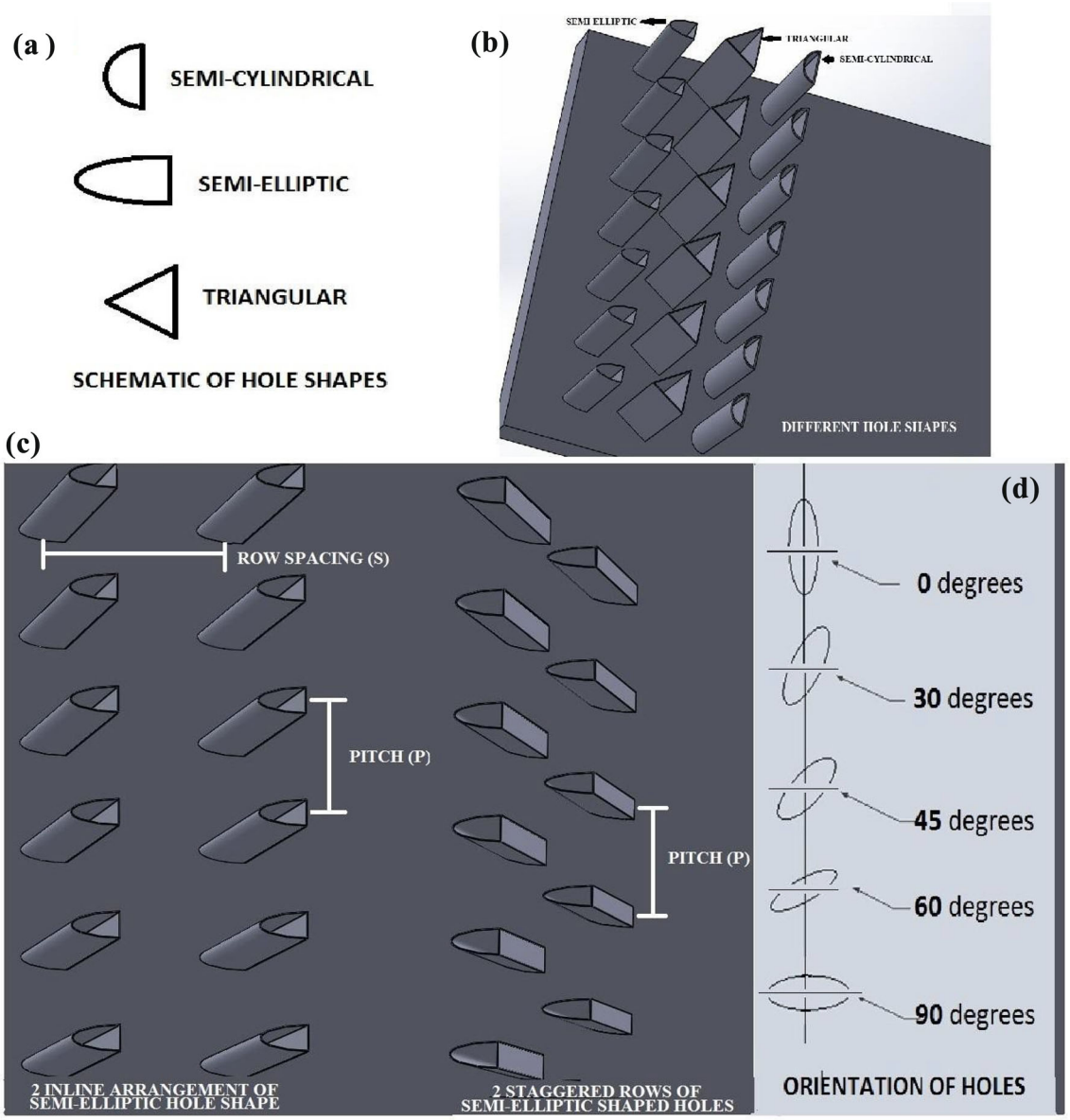

Figure 2. Schematic and modelled view of different CIH geometries and their orientations.

Table 1. Boundary conditions.

Boundary conditions	Values
Free-stream inlet velocity	15 m/s
Free-stream inlet temperature	600 K
Density ratio	~1.0
Coolant inlet temperature	300 K

Table 2. Coolant inlet velocities with blowing ratios.

S. No.	Blowing ratio (M)	Coolant inlet velocity (m/s)
1.	0.67	10
2.	1.00	15
3.	1.33	20
4.	1.67	25

Table 3. Various grid sizes for different meshes.

Grid	Cells	Faces	Nodes
Coarse	328161	1012327	347496
Medium	1218503	3722717	1265081
Fine	3818611	11548111	3911868

3. Results and discussion

3.1 *Validation of the computational model*

The computational results obtained for a single cylindrical CIH are evaluated with the experimental results reported by Yuen *et al* [6] to validate the designed simulation model. The performance of different CIH geometries (semi-cylindrical, triangular and semi-elliptic) for ηfc is measured in the centerline (ηcl) and spatially averaged adiabatic (ηsa) film cooling effectiveness. For all the cases, the non-dimensional temperature profiles are also plotted. Figure 3(b) represents the comparison and validation of the obtained computational results with the reported experimental results. Figure 3(b) presents the validation only at M=1.00; however, the validation is done at all the blowing ratios. As presented in figure 3(b), the ηcl values agree well with the experimental results. A small disparity can be observed in a small near-CIH region (x/D <5.0). The overall deviation of the obtained effectiveness values from the experimental data is 5.7% approximately. This observed difference can be attributed to the fact that in a computational simulation model, coolant jet height is not considered which leads to improved lateral dispersal of the coolant and consequently higher film ηfc values in the near CIH-region (x/D <5.0).

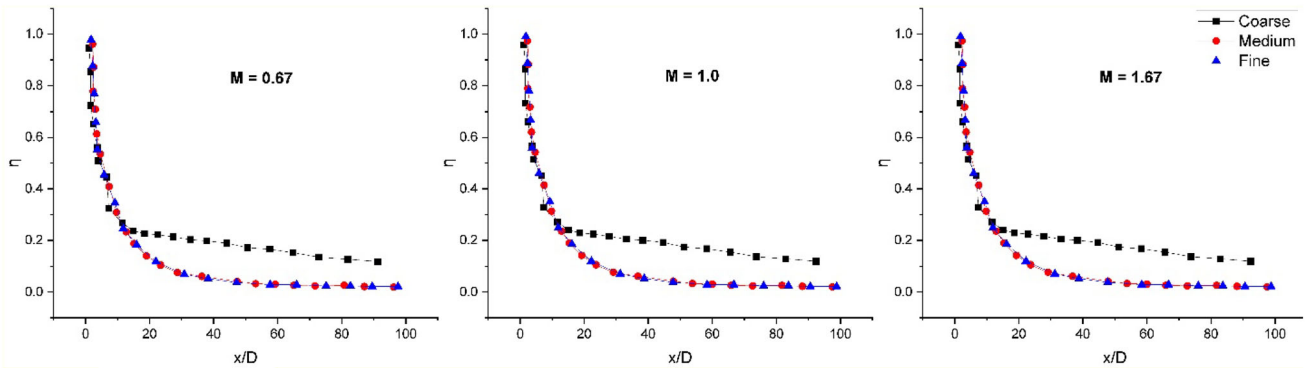

(a) Grid Independence Test over all the Blowing ratios M = 0.67, 1.0 and 1.67)

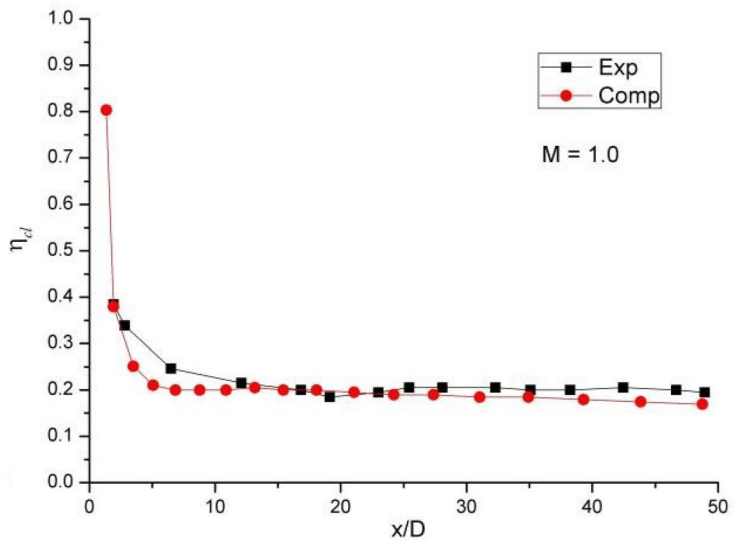

(b) Validation with the experimental work [6].

Figure 3. (**a**) Grid Independence Test over all the Blowing ratios M = 0.67, 1.0 and 1.67). (**b**) Validation with the experimental work [6].

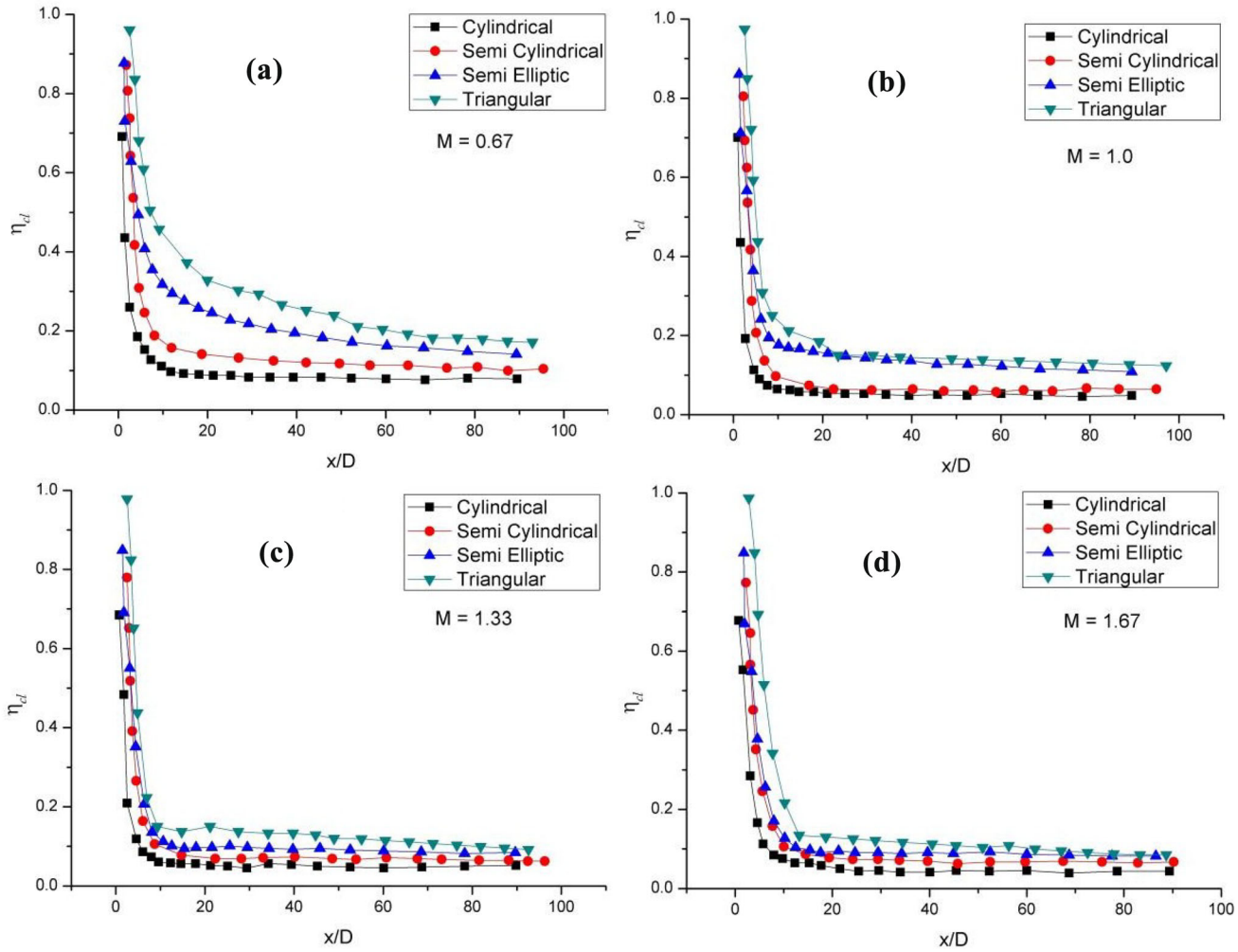

Figure 4. The *ηcl* for different CIH geometries with varying blowing ratios, (**a**) M = 0.67 (**b**) M = 1.0 (**c**) M = 1.33 (**d**) M = 1.67.

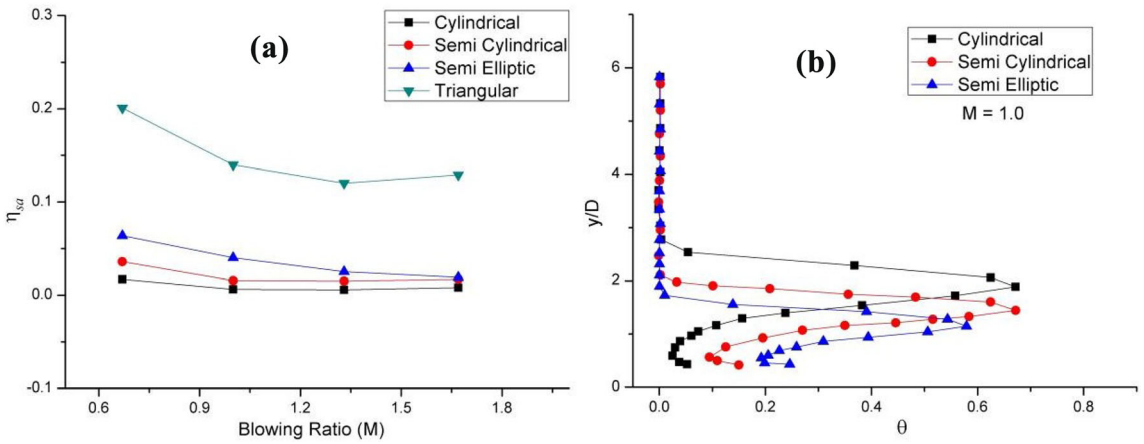

Figure 5. (**a**) Variation of *ηsa* with M; (**b**) Variation of θ with y/D for all shapes.

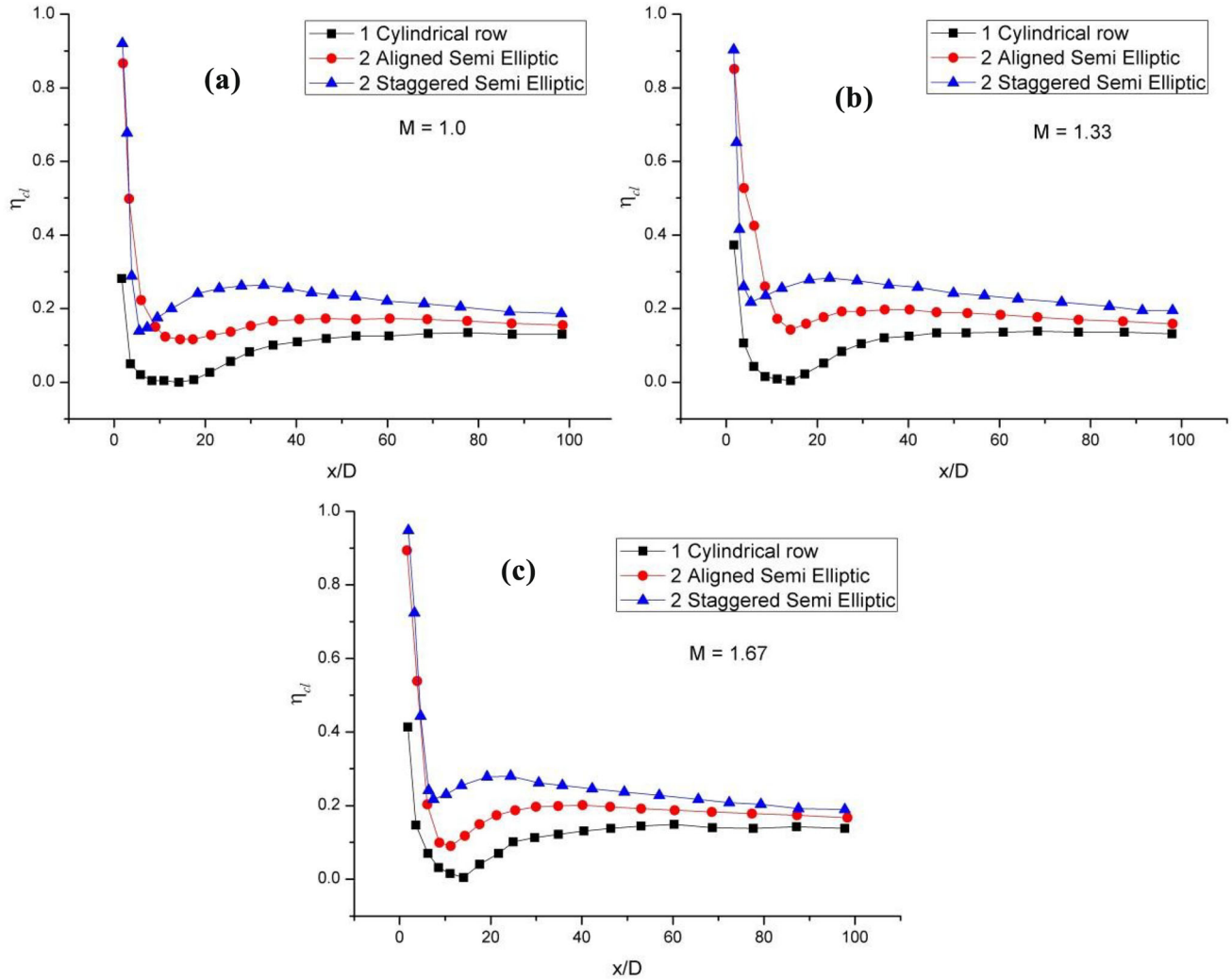

Figure 6. The ηcl for multiple rows of CIHs at different blowing ratios, (**a**) M = 1.0 (**b**) M = 1.33 (**c**) M = 1.67.

3.2 *Different geometry CIHs (Single)*

Figure 4 depicts the ηcl values for semi-cylindrical, triangular, and semi-elliptic CIHs compared with cylindrical CIH. In all the cases, the triangular CIH delivered the best results for ηfc, however, both the semi-geometries performed well than the cylindrical CIHs in terms of coolant's mass flow rate. At low M values (0.67, 1.00), a higher ηcl values are obtained for triangular and semi-elliptic CIHs rather than the other two geometries (figure 4(a) and 4(b)).

The semi-cylindrical CIH has almost the same effectiveness values as a cylindrical coolant injection hole. At higher M values, i.e., 1.33 and 1.67 (figure 4(c) and 4(d)), slightly higher ηcl values are obtained in the near-CIH region of triangular and both semi-geometries CIHs than that in a cylindrical one. This behaviour can be attributed to better lateral dispersal of the coolant from the straight edges of the geometry. Although the triangular CIH gives better effectiveness values in all the cases, the semi-elliptic CIH tends to utilize $\sim$50% of the coolant mass flow rate per unit area as the triangular coolant injection hole.

Spatially averaged film cooling effectiveness for various CIH geometries are presented in figure 5(a) to represent the effect of M values and the CIHs geometry. For cylindrical and semi-cylindrical CIHs, the ηsa values decrease up to a blowing ratio of 1.00, whereas the value keeps on decreasing until M=1.33 for the other two geometries [15]. Among all the geometries, the highest values of ηsa are deliver by the triangular CIH. However, the semi- elliptic CIH performs better than the semi-cylindrical and cylindrical CIH geometries when it comes to coolant consumption.

Non-dimensional temperature profiles are plotted to explain the concept of coolant jet heights. A fewer coolant jet heights are desirable for achieving higher effectiveness values [16]. As shown in figure 5(b), both the semi-geometries have fewer coolant jet heights and consequently deliver higher effectiveness values. Only one case

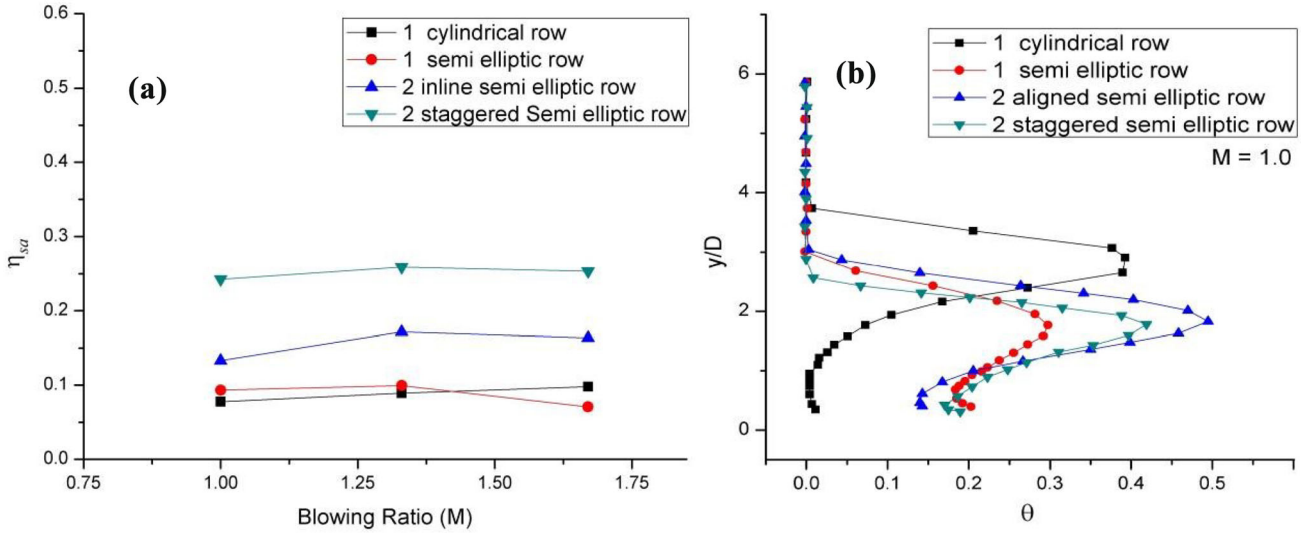

Figure 7. (**a**) Variation of *ηsa* with M; (**b**) Variation of θ with y/D for multiple rows.

(*M*=1.00) is reported in the present study, as other cases exhibit a similar nature of the curve.

In figure 5(b), θ=0.0 implies free-stream temperature (600 K) while θ=1.0 implies coolant temperature (300 K) without mixing with the free-stream. Figure 5(b) suggests that the semi- elliptic CIHs have the minimum while the cylindrical CIHs have maximum coolant jet mean height. The coolant jet height is observed to increase with increasing blowing ratios. No coolant was observed above the *y/D* (the ratio of lateral distance from the hole center to hole diameter) value of 2.5 stating the ineffectiveness of the colling scheme at that distance.

3.3 *Arrangement of CIHs/rows*

The semi-geometries have been favored over the triangular CIH for injecting coolant from numerous rows of coolant injection holes since they perform equivalent at almost ∼50% of the coolant mass flow rate. The comparative results of a single row of cylindrical CIHs with two staggered rows of semi-elliptic and two aligned rows of semi-elliptic CIHs have been presented in figure 6. Both semi-geometric CIHs exhibit superior values of *ηcl* at all *x/D* values for all *M* values (1.0 - 1.67) as like a scheme with single CIH.

There is a sudden decrease in *ηfc* in the near-CIH region due to coolant jet lift-off. This jet lift- off is least for staggered row cases in contrast to others since the decrement of the *ηfc* is minimum. The *ηcl* values for aligned semi-elliptic rows is superior at M= 1.0 and 1.33, up till *x/D*<10. This increment can be attributed to the presence of additional coolant from the upstream CIHs row [17]. Apart from this, the staggered rows of CIHs exhibit much higher *ηcl* values at all other *x*/D values (>10). This phenomenon occurs due to the lateral dispersal of the coolant on the flat plate surface, and no room is left for the free-stream flow to penetrate between CIHs of downstream staggered rows. Also, the reattachment of the coolant jet to the flat surface starts at around *x/D*=7 for the staggered case, in contrast to others. This behaviour can be attributed to the arrangement of the CIHs, as the lateral distance between the CIHs of both the rows is dependent of each other.

Figure 7(a) shows the *ηsa* for all CIH geometries at all *M* values. The *ηsa* values for single row of semi-cylindrical and cylindrical CIHs are found to be almost similar. For two rows of staggered semi-elliptic CIHs case, the effectiveness values are nearly double to that of the single row of cylindrical coolant injection holes. The values of θ for all CIH arrangements has been presented at all values of M. The maximum θ value at a particular location gives the mean jet height of the coolant at that point [18]. All the configurations show that the coolant jet height increases with the increase of blowing ratio. Figure 7(b) presents the various CIH arrangements for M=1.0 only. It is evident from figure 7(b) that the amalgamation of coolant into the free-stream flow is the minimum for the case of semi-geometry row as they have much inferior coolant jet heights than the row of cylindrical coolant injection holes. The minimum coolant jet heights were observed in the semi-elliptic two staggered rows show, and hence for all the cases, they have the maximum effectiveness values. As can be seen from high θ values for all semi-elliptic cases, the presence of coolant is very high at low *y/D* values.

3.4 *Compound angle orientations*

Various hole arrangements for single and multiple rows have been evaluated at fixed values of orientation angle (β),

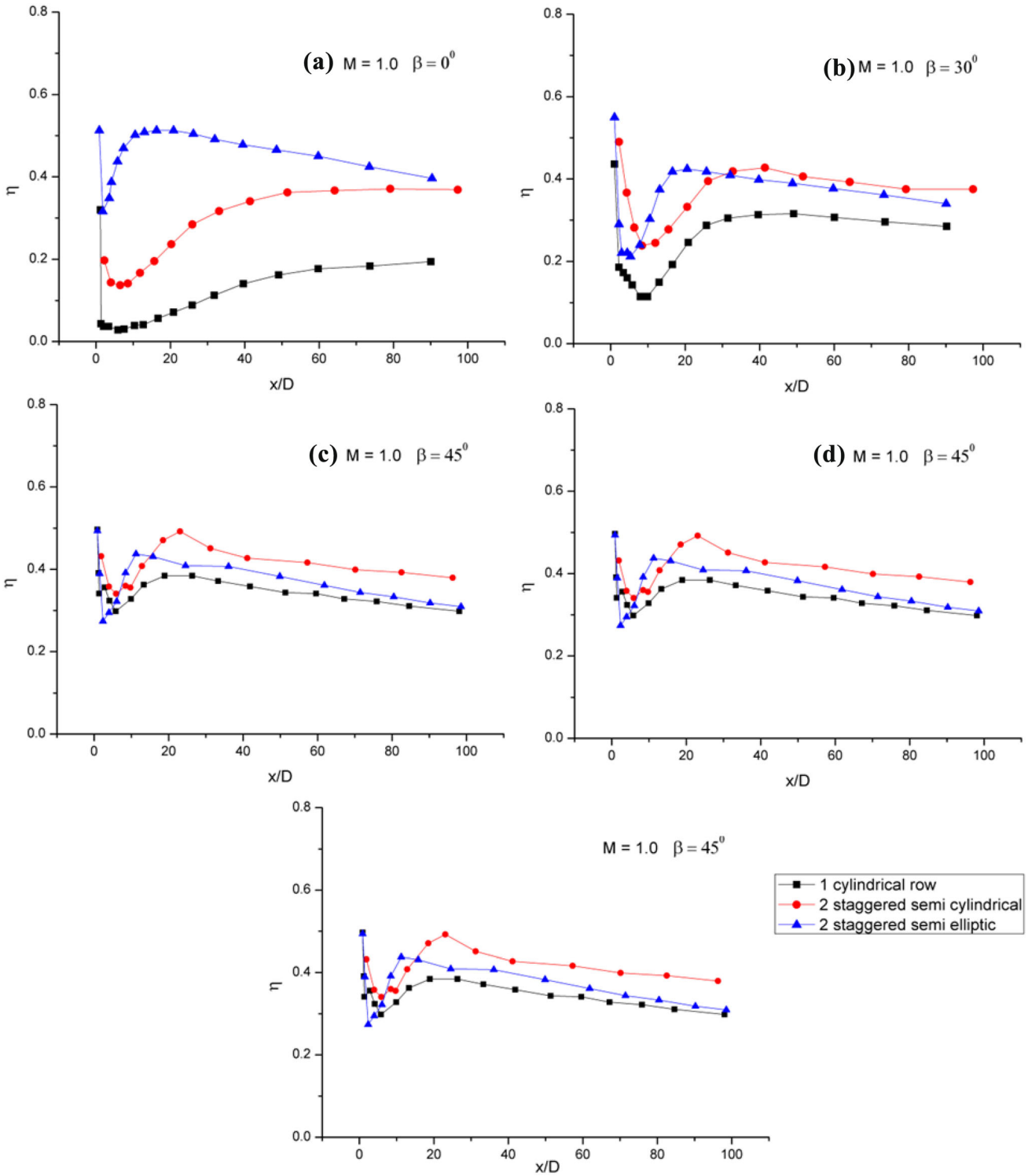

Figure 8. The *ηcl* values for Multiple Rows with various orientation angles (*β*), (**a**) 0°, (**b**) 30°, (**c**) 45°, (**d**) 60°, (**e**) 90°.

which vary from 0° to 90°. One row of cylindrical CIHs has been compared with the two staggered rows of semi-cylindrical and semi-elliptic CIHs at a blowing ratio of 1.00. The pitch-to-diameter ratio (P/D) for cylindrical and semi-geometric CIHs is 5. Much higher values of ηcl have been achieved at all the compound angles for staggered rows of semi-geometric CIHs than the single row of cylindrical coolant injection holes. While comparing

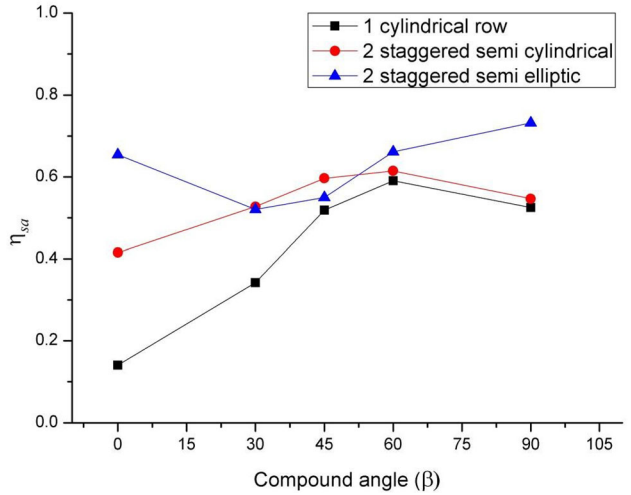

Figure 9. Variation of *ηsa* with varying orientation angles.

between the staggered rows of semi-geometric CIHs, the semi- elliptic CIHs deliver much higher effectiveness values than the other two configurations. As shown in figure 8(a) for β = 0°, there is a sharp increase in the effectiveness just after the near-CIH region, which might result from abrupt reattachment of coolant jet with the surface. For β=30°, as shown in figure 8(b), the ηcl values for the semi-elliptic case is much higher at 8≤ x/D≤ 25.

However, for both the semi-geometries, the *ηcl* values are higher than that of the cylindrical row of coolant injection holes. On comparing the results of *β*=0° and *β*=30°, it is inferred that the difference in the *ηcl* values has been reduced. For *β*=45°, the semi-cylindrical row of CIHs shows higher effectiveness than the other two configurations of the row of CIHs in the streamwise region of 15≤*x*/D≤100 (figure 8(c)). However, from figure 8(d), for *β*=60°, the staggered rows of semi geometries have almost the same *ηcl* values but are far more effective than the cylindrical row of coolant injection holes. From figure 8(e), at *β*=90°, the *ηcl* values from each case of staggered rows of semi-geometric CIHs is much higher than that of the cylindrical CIHs after the streamwise region of 1≤*x*/*D*≤ 5. Again, the semi-elliptic CIH gives much higher *ηcl* values up to *x*/*D*=25, after which it becomes almost equal to the values from the semi-cylindrical case.

The *ηsa* has been plotted for all the hole configurations at all orientation angles, as shown in figure 9. The *ηsa* increases with an increase in *β* up to 60° for the cylindrical and semi- cylindrical case while it decreases on further increasing the angle. This is because the orientation is reducing the lateral spreading of the coolant and hence effectiveness values. For semi-elliptic CIHs, the *ηsa* decreases with an increase in *β* up to 30° and an insignificant increase till *β*=45°, while it further increases with an increase in the angle. At *β*=0°, the two staggered semi-elliptic CIHs show 400-600% increment than the other two configurations. There is a significant increase of ∼200% overall in the *ηsa* values from rows of semi-elliptic CIHs than the row of cylindrical coolant injection holes.

4. Conclusion

Various geometries, i.e., cylindrical, triangular, semi-cylindrical and semi-elliptic, for coolant injection holes have been reported and compared to each other to obtain better performance in terms of centerline and spatially averaged film cooling effectiveness. Reduced coolant jet height was observed for the triangular and semi-elliptic coolant injection hole geometries, resulting in higher centerline film cooling effectiveness. Also, the semi-elliptic coolant injection hole is far more advantageous as the coolant mass flow rate is only half that required by the cylindrical coolant injection hole for the same blowing ratio. Higher effectiveness values are obtained because of the lowest coolant jet heights in this case. Further, adding more rows of coolant injection holes gave better results. It is concluded that for a single CIH configuration, the semi-elliptic and triangular CIHs increased the *ηcl* by ∼66.67% up to *x*/*D*=50 and ∼50% up to *x*/*D*=100 at lower *M* values (0.67 and 1.00). At higher values of *M* (1.33 and 1.67), this increment is ∼100% up to *x*/*D*=50 and ∼50% up to *x*/*D*=100. For *ηsa*, a significant increment of ∼200% in triangular CIH while ∼60% for the semi-elliptic CIH is observed for all blowing ratios. For the multiple row arrangements, the two staggered row configuration showed promising results with increment in *ηcl* by ∼77% up to *x*/*D*=50 and ∼54% up to *x*/*D*=100. In this case, the observed value of *ηsa* was ∼150% more than the conventional cases. For orientation of CIHs, results were analyzed over the different rows arrangements, and it was found that the two staggered row configuration at 0° delivered the highest effectiveness values. An increment of ∼177% was observed up to *x*/*D*=50 while ∼100% up to *x*/*D*=100. A significant increase of about ∼200% in the spatially averaged effectiveness from rows of semi-elliptic CIHs rather than the single row of cylindrical CIHs was observed. It is suggested that the film cooling effectiveness might be due to the early merging of coolant jets from the adjacent CIHs and nearby rows (staggered configuration) due to the spanwise diffusion of the cooling fluid increases significantly for staggered row configuration. The results show a substantial decrement in film cooling effectiveness for very low blowing ratios because of high turbulence levels. Low and high turbulence levels have similar effects on film cooling effectiveness for higher blowing ratios. The present study concludes that two staggered rows of semi-elliptic CIHs can be used for film cooling with a compound angle of 0° to achieve comparatively higher film cooling effectiveness.

5. List of Symbols

Tw	Adiabatic wall temperature, K
T∞	Free stream temperature, K
Tc	Coolant inlet temperature, 300 K
u=[u v]	Steady-state velocity field
ρ	Density
Cp	Specific heat capacity
T	Steady-state temperature
k	Conductivity
Q	Heat source
k	Turbulent kinetic energy
ε	Turbulence dissipation rate
μ_T	Turbulent viscosity

Funding This research received no specific grant from any funding agency in the public, commercial, or not-for-profit sectors.

Declarations

Competing interest The authors declare that they have no known competing financial interests or personal relationships that could have appeared to influence the work reported in this paper.

References

[1] Li J, Yan X, He K and Goldstein R J 2021 Implementation of rectangular vortex generator pairs to improve film cooling effectiveness on transonic rotor blade endwall. *J. Eng. Gas Turbines Power.* 143(9): 091022

[2] Wang N, Shiau C C, Han J C, Xu H and Fox M 2019 Turbine vane endwall film cooling from mid-chord or downstream rows and upstream coolant injection. *Int. J. Heat Mass Transf.* 133: 247–255

[3] Azzi A and Jubran B A 2007 Numerical modelling of film cooling from converging slot-hole. *Heat Mass Transf.* 43(4): 381–388

[4] Bunker R S 2005 A review of shaped hole turbine film-cooling technology. *J. Heat Transfer.* 127(4): 441–453

[5] Goldstein R J, Eckert E R and Ramsey J W 1968 Film cooling with injection through holes: adiabatic wall temperatures downstream of a circular hole. *J. Eng. Power.* 90(4): 384–393

[6] Yuen C H and Martinez-Botas R F 2003 Film cooling characteristics of a single round hole at various streamwise angles in a crossflow: Part I effectiveness. *Int. J. Heat Mass Transf.* 46(2): 221–235

[7] Yuen C H and Martinez-Botas R F 2003 Film cooling characteristics of a single round hole at various streamwise angles in a crossflow: Part II: Heat transfer coefficients. *Int. J. Heat Mass Transf.* 46(2): 237–249

[8] Chen P, Gao H, Li X, Ren J and Jiang H 2018 Effects of endwall 3D Contouring on film cooling effectiveness of cylindrical hole injections at different locations on vane endwall. In: *Proceedings of the ASME Turbo Expo 2018: Turbomachinery Technical Conference and Exposition. Volume 5C: Heat Transfer. Oslo, Norway.* 51104: V05CT19A031

[9] Wang T and Li X 2008 Mist film cooling simulation at gas turbine operating conditions. *Int. J. Heat Mass. Transf.* 51(21–22): 5305–5317

[10] Guangchao L, Huiren Z and Huiming F 2008 Influences of hole shape on film cooling characteristics with CO2 injection. *Chinese J. Aeronaut.* 21(5): 393–401

[11] Dellimore K H, Marshall A W and Cadou C P 2010 Influence of compressibility on film-cooling performance. *J. Thermophys. Heat Transf.* 24(3): 506–515

[12] Wright L M, McClain S T and Clemenson M D 2010 Effect of density ratio on flat plate film cooling with shaped holes using PSP. *J. Turbomach.* 133(4): 041011

[13] Baheri S, Tabrizi S P and Jubran B A 2008 Film cooling effectiveness from trenched shaped and compound holes. *Heat Mass Transf.* 44(8): 989–998

[14] Asghar F H and Hyder M J 2010 Computational study of film cooling effectiveness for a comparison of cylindrical, square and triangular holes of equal cross-sectional area. *Mehran Univ. Res. J. Eng. Technol.* 29(4): 541–556

[15] Jindal P, Agarwal S, Sharma R P and Roy A K 2017 Numerical investigation of film cooling enhancement using staggered row mixed hole arrangements. *J. Therm. Sci. Eng. Appl.* 9(2): 021007

[16] Shiau C C, Sahin I, Wang N, Han J C, Xu H and Fox M 2019 Turbine vane endwall film cooling comparison from five film-hole design patterns and three upstream injection angles. *J. Therm. Sci. Eng. Appl.* 11(3): 031012

[17] Li J, Yan X and He K 2020 Effect of non-axisymmetric endwall profiling on heat transfer and film cooling effectiveness of a transonic rotor blade. *J. Turbomach.* 142(5): 051006

[18] Bu H, Guo Z, Song L and Li J 2021 Effects of cooling configurations on the aerothermal performance of a turbine endwall with jet impingement and film cooling. *J. Turbomach.* 143(6): 061013

Springer Nature or its licensor (e.g. a society or other partner) holds exclusive rights to this article under a publishing agreement with the author(s) or other rightsholder(s); author self-archiving of the accepted manuscript version of this article is solely governed by the terms of such publishing agreement and applicable law.